

Experimental analysis of particle and fluid motion in ac electrokinetics

Dazhi Wang, Marin Sigurdson, Carl D. Meinhart

Abstract An ac electric field is applied to induce particle and fluid motion in a wedge-shaped microchannel. Micron-resolution particle image velocimetry (μ -PIV) is used to determine spatially resolved particle velocity and fluid velocity fields. Under steady-state conditions, the particles experience a balance between dielectrophoretic forces induced by the nonuniform electric field and Stokes' drag forces due to viscous interactions with the fluid. The particle velocity is therefore different from the fluid velocity because of dielectrophoresis. A variant of μ -PIV, two-color μ -PIV, is developed and used to uniquely determine the fluid velocity from the observation of particles without a priori knowledge of the electrical properties. This technique is used to explore ac electrokinetically generated fluid motion. A series of voltage levels at fixed frequency are applied to the wedge-shaped electrodes. The dependency of fluid velocity on applied voltage at different regions in the flow is obtained by fitting power-law curves. This is used to determine the underlying physical phenomena associated with ac electrokinetics. We found that both electrothermal effects and ac electroosmosis are important for the current experimental conditions. However, the electrothermal effect is dominant in the bulk fluid.

1

Introduction

In the presence of nonuniform electric fields, particles in a suspension experience dielectrophoretic (DEP) forces (Jones 1995). This force can move a particle towards areas of high-field or low-field strength, depending on the difference of electrical properties between the particles and the suspending medium. These properties are a function of the frequency of the applied signal. Using microfabricated

devices, manipulation of particles using DEP forces can be achieved in microscale channels on a chip with relatively small voltages. Dielectrophoresis has important applications in biological procedures, such as detecting, manipulating and separating bioparticles like cells, viruses, proteins and DNA (Bakewell et al. 1998; Morgan et al. 1999; Yang et al. 1999a, 1999b; Sigurdson et al. 2002).

While a nonuniform ac electric field can move suspended particles using dielectrophoretic forces, it can also move the fluid through the electrothermal effect or ac electroosmosis (Ramos et al. 1998, 2000; Green et al. 2000; Meinhart et al. 2003). Green et al. (2000) has conducted measurements of particle motion under the influence of nonuniform ac electric fields. Nonuniform electric fields produce spatially varying power densities in the fluid and therefore nonuniform temperature fields in the fluid, leading to local changes in conductivity and permittivity. The applied electric field interacts with gradients of conductivity and permittivity, giving rise to electrothermal forces in the liquid. In addition, ac electric fields produce double layers at the interface between the electrodes and the fluid. AC electroosmosis occurs when the bulk fluid is put in motion by the action of the tangential component of the electric field on the induced double layers. Both the electrothermal effect and ac electroosmosis can be used to pump fluids or to turn on and off vortices in microfluidic devices without moving parts (Brown et al. 2001; Studeer et al. 2002). These can be used to actively separate, mix, or direct biological particles (Wong et al. 2003a, 2003b).

Micron-resolution particle image velocimetry (μ -PIV) is a unique technique that allows detailed measurements of two-dimensional particle velocity and fluid velocity in microfluidic devices with spatial resolutions approaching 1 μm (Meinhart et al. 1999, 2000a, 2000b; Cummings 2000). Typically, μ -PIV measures the fluid velocity by tracking the motion of fluorescent particles with an assumption that the small particles faithfully follow the fluid flow. In the current experiment, the particle velocity is different from the underlying fluid velocity, due to the DEP forces on the particles induced by the applied electric fields. The dielectrophoretic mobilities of particles and the fluid velocity can be measured using two-color μ -PIV (Meinhart and Wang 2001; Meinhart et al. 2003).

In this paper, we combine two-color fluorescent imaging with micron-resolution PIV to measure fluid velocity fields within a microfluidic device, subject to nonuniform ac electric fields. We compare the relative importance of the electrothermal effect to ac electroosmosis under certain experiment conditions.

Received: 17 October 2003 / Accepted: 3 August 2004
Published online: 2 December 2004
© Springer-Verlag 2004

D. Wang, M. Sigurdson, C. D. Meinhart (✉)
Department of Mechanical & Environmental Engineering,
University of California, Santa Barbara, CA 93106, USA
E-mail: meinhart@engineering.ucsb.edu

This work is supported by DARPA/ARMY DAAD 19-00-1-0400, DARPA/Air Force F30602-00-2-0609, NSF CTS-9874839 and NSF ACI-0086061.

AC electrokinetics

AC electrokinetics refers to the movement of particles and/or fluid induced by ac electric fields. The particles and the fluid may affect each other through viscous interaction. If the volume fraction of the particles is sufficiently low, the effect of the particles on the fluid is negligible.

2.1

Particle motion

Under the influence of nonuniform electric fields, a particle in an aqueous medium experiences dielectrophoretic force and drag force. These forces are approximately balanced in steady-state, non-inertial flows, such that

$$\vec{F}_{\text{DEP}} + \vec{F}_{\text{D}} = 0, \quad (1)$$

where \vec{F}_{DEP} and \vec{F}_{D} are the forces due to DEP and Stokes' drag, respectively.

The time-averaged dielectrophoretic force on a homogeneous spherical particle is (Jones 1995)

$$\vec{F}_{\text{DEP}} = 2\pi\epsilon_m r^3 \text{Re}\{K\} \nabla |\vec{E}_{\text{rms}}|^2 \quad (2)$$

where ϵ_m is the permittivity of the medium, r the particle radius, E_{rms} the root mean square of the ac electric field and K the Clausius-Mossotti factor given by

$$K = \frac{\epsilon_p^* - \epsilon_m^*}{\epsilon_p^* + 2\epsilon_m^*}, \quad (3)$$

where $\epsilon^* = \epsilon - j\sigma/\omega$ is the complex permittivity, σ is the electrical conductivity, and subscripts p and m represent the particle and the suspending medium, respectively. The complex permittivity is a strong function of the frequency, ω , of the applied signal.

The sign of the real part of the Clausius-Mossotti factor, $\text{Re}\{K\}$, defines positive ($\text{Re}\{K\} > 0$) and negative ($\text{Re}\{K\} < 0$) dielectrophoresis. $\text{Re}\{K\}$ ranges from -0.5 to 1 . The particles are moved toward the electric field intensity maxima by positive DEP forces and toward the minima by negative DEP forces.

The particles also experience drag forces due to viscous interactions with the fluid. In the current experiments, the Reynolds number is $Re = 0.005$, much less than 1 , with the characteristic fluid velocity of $100 \mu\text{m/s}$ and the characteristic length scale of $50 \mu\text{m}$. The flow motion in the microchannel is not uniform, but we can assume the fluid velocity is uniform far from a particle, considering the diameter of the particle is only $1 \mu\text{m}$. The drag force on a spherical particle follows Stokes' law

$$\vec{F}_{\text{D}} = 6\pi\mu r(\vec{u}_f - \vec{u}_p), \quad (4)$$

where μ is the viscosity of the medium, \vec{u}_f is the fluid velocity and \vec{u}_p is the particle velocity.

2.2

Fluid motion

The motion of incompressible fluid is governed by Stokes' equation, where the inertia terms are neglected, due to the near-zero Reynolds number,

$$\mu \nabla^2 \vec{u}_f - \nabla p + \vec{f} = 0, \quad (5)$$

and the mass-conservation equation

$$\nabla \cdot \vec{u}_f = 0, \quad (6)$$

where p is the pressure and \vec{f} is the body force.

In our experiments, the solid volume fraction of the working suspension is 0.07% . Subject to ac electric fields, the fluid motion could be caused by the electrothermal effect, ac electroosmosis, or other unknown mechanisms.

2.2.1

Electrothermal effect

Wedge-shaped electrodes produce nonuniform electric fields, resulting in nonuniform power density in the fluid and in turn, nonuniform temperature fields. Neglecting convective effects, which is reasonable at the microscale (Ramos et al. 1998), at steady state the temperature equation is obtained by balancing Joule heating with thermal diffusion

$$k \nabla^2 T + \sigma E^2 = 0, \quad (7)$$

where σ is the conductivity, and σE^2 represents the power density generated in the fluid by Joule heating from the applied electric fields. The electric field can be written in terms of the electric potential, $E = -\nabla V$, where the applied potential V in a charge neutral fluid obeys Laplace's equation, $\nabla^2 V = 0$.

The properties of the suspending medium are functions of temperature. The spatially varying temperature field leads to variation in properties such as charge density, electrical conductivity and permittivity. The existence of temperature gradients in fluid may result in natural convection. The Rayleigh number $Ra = (g\beta\Delta T L^3/\nu^2)Pr$ indicates the importance of natural convection. Here β is the thermal expansion coefficient, ΔT is the temperature difference, L is the length scale, ν is the kinematic viscosity and Pr is the Prandtl number. For water at 20°C , $\beta = 2.1 \times 10^{-4} \text{K}^{-1}$, $\nu = 1.0 \times 10^{-6} \text{m}^2/\text{s}$, $Pr = 7.1$ (Kundu and Cohen 2002). The length scale is the channel depth, $L = 550 \times 10^{-6} \text{m}$. The maximum temperature rise is about 3°C at $14 V_{\text{rms}}$ (according to our numerical simulations; data not shown). Therefore, $Ra = 7.3$, far less than the critical value of $1,708$ at which the natural convection would occur, indicating that the natural convection is negligible (Deen 1998).

The electric fields interact with the gradients of permittivity and conductivity, giving rise to the electrothermal force that induces fluid motion. This phenomenon is termed the electrothermal effect. The time-averaged electrothermal force is expressed as (Ramos et al. 1998)

$$\vec{f}_E = -\frac{1}{2} \left[\left(\frac{\nabla \sigma}{\sigma} - \frac{\nabla \epsilon}{\epsilon} \right) \cdot \vec{E}_0 \frac{\epsilon \vec{E}_0}{1 + (\omega\tau)^2} + \frac{1}{2} |\vec{E}_0|^2 \nabla \epsilon \right], \quad (8)$$

where E_0 is the amplitude of the applied electric field, ω is the applied frequency, and $\tau = \epsilon/\sigma$ is the charge relaxation time. The gradients of conductivity and permittivity are related to temperature by $\nabla \epsilon = (\partial\epsilon/\partial T)\nabla T$ and $\nabla \sigma = (\partial\sigma/\partial T)\nabla T$.

Equations (5), (6), (7), (8) describe the fluid motion caused by the electrothermal effect. The relation between the fluid velocity and the applied voltage can be estimated by order-of-magnitude analysis of these equations. It can be deduced that $u_f \sim f_E$ from Eq. (5), $\Delta T \sim V^2$ from Eq. (7) and $f_E \sim (\Delta T)V^2$ from Eq. (8). Consequently, if the fluid motion is induced by electric fields due to the electrothermal effect, the magnitude of fluid velocity is proportional to the 4th power of the applied voltage, such that

$$u_f \sim V^4. \quad (9)$$

2.2.2 AC electroosmosis

Similar to dc electroosmosis, fluid motion can also be induced by ac electric fields (Ramos et al. 1998, 2000; Green et al. 2000). Electrical double layers can form at the interface between the electrodes and the fluid. The ions in the double layers are moved by electrical forces due to the non-zero tangential components of the electric fields at the edge of the double layer, which induce the bulk fluid motion. The sign of the ions in the double layers is always opposite to that of the charges on the corresponding electrode surfaces, which produces a cumulative effect under ac electric fields, and therefore results in steady-state fluid motion (Morgan and Green 2003).

The scale of the double layer width is of order 1–10 nm, whereas the characteristic length of the channels is of order 100 μm in the present investigation. Consequently, the bulk fluid motion due to ac electroosmosis can be described by Eqs. (5) and (6) with body force $\vec{f} = 0$ and a finite velocity specified as the boundary condition at the electrode surface. The fluid velocity due to ac electroosmosis at the electrode surfaces is proportional to the square of the applied voltage (Green et al. 2000)

$$u_f \sim V^2. \quad (10)$$

3 Experiment details

3.1 $\mu\text{-PIV}$ method

Micron-resolution particle image velocimetry ($\mu\text{-PIV}$) has been developed to obtain quantitative measurements of spatially resolved fluid motion at microscale (Santiago et al. 1998; Meinhart et al. 1999, 2000a, 2000b; Cummings 2000; Meinhart and Wang 2001). This technique measures fluid motion by measuring the motion of fluorescent micron-sized tracing particles suspended in a transparent working fluid. Typically, it is assumed that the particles faithfully follow the fluid.

In the current experiment, particle images are recorded using an epi-fluorescence microscope (ECLIPSE E600FN, Nikon, Melville, NY) and a 1280 \times 1024 \times 12-bit CCD camera (C7300-10-12NR, Hamamatsu, Tustin, CA). Figure 1 shows a schematic of the $\mu\text{-PIV}$ system. Continuous illumination light is provided by a mercury arc lamp, filtered by an excitation filter and transferred to the microfluidic device through the objective lens. The fluorescently dyed

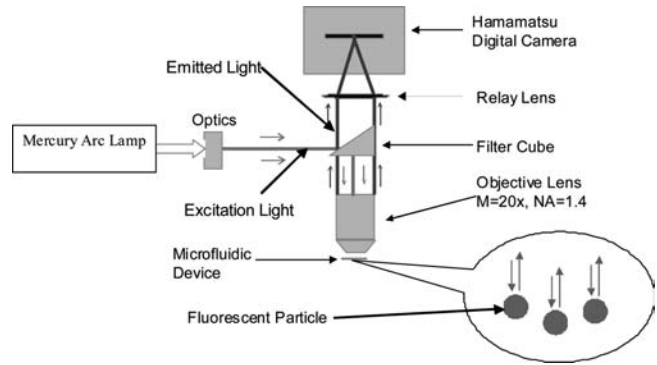


Fig. 1. Schematic view of the $\mu\text{-PIV}$ system

particles in the fluid are excited and emit fluorescent light. The emitted light is passed through a barrier filter and delivered to the CCD camera. In the microscope, an infrared filter (HA50, Nikon, Melville, NY) is inserted into the optical path of the illumination source to absorb IR heat from the mercury arc lamp. In addition, the test section is only exposed to the illumination light for 30s during the particle image velocimetry. Therefore, we assume that the illumination heating in the fluid is negligible. Time-sequences of images are correlated and then ensemble-averaged to obtain 2-D velocity fields, following the technique developed by Meinhart et al. (2000b).

3.2 Two-color $\mu\text{-PIV}$

In the presence of nonuniform electric fields, dielectrophoretic forces cause the particle velocity to differ from the fluid velocity. However, if particle velocity fields are measured using two sets of electrically similar particles, but with two distinct sizes, under the same electric field and flow conditions, the fluid velocity can be uniquely determined. In order to distinguish between two different-sized sets of particles in PIV measurement, the different-sized particles are labeled with different-colored fluorescent dye. Figure 2 shows how the choice of the appropriate filter allows selective recording of either the large or the small

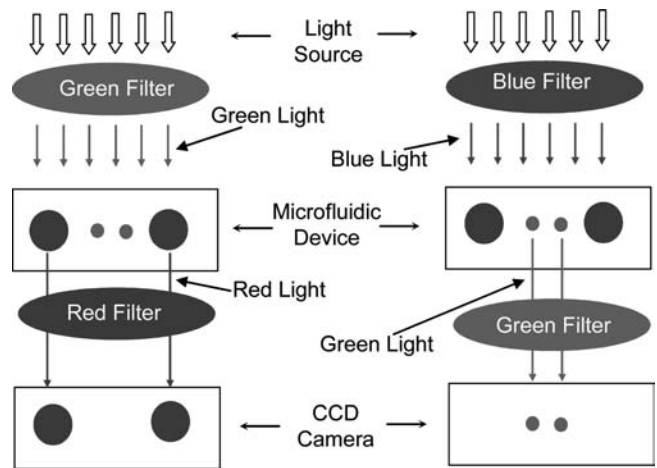


Fig. 2. Schematic of the process of the measurements using two-color $\mu\text{-PIV}$. Two different-sized particles with different colors can be recorded by adjusting the filter cube apparatus. This minimizes disturbances of the fluid experiment

Table 1. Spectral properties of fluorescent particles

Specified color	Excitation maxima (nm)	Emission maxima (nm)	Stokes shift (nm)
Green	468 (blue)	508 (green)	40
Red	542 (green)	612 (red)	70

particles by the CCD camera. When the filter cube assembly is positioned so that the green excitation and red barrier filters are activated, only the larger 1 μm red fluorescent particles are recorded. Positioning the filter cube assembly to activate the blue excitation and green barrier filters allows only the small 0.7 μm green fluorescent particles to be recorded by the CCD camera. Therefore, the flow experiment is not disturbed during the process of recording the images of different-sized particles.

The spectral characteristics of the fluorescent particles are listed in Table 1 and are available from Duke Scientific Corp. (Palo Alto, CA).

The corresponding filter cubes were bought from Chroma Technology Corp. (Rockingham, VT). The filter cube for the red particles consists of an exciter D525/20 (bandpass filter, centered at 525nm, 20nm width) and an emitter E550LP (long-pass filter, cutoff at 550nm). The filter cube for the green particles consists of an exciter HQ450/50 (bandpass filter, centered at 450nm, 50nm width), a dichroic Q480LP (long-pass filter, cutoff at 480nm) and an emitter HQ510/50 (bandpass filter, centered at 510nm, 50nm width). In order to test the degree of overlap between the two filter schemes, two images were taken through each filter cube of the green and red particles fixed to a glass slide, and are shown in Fig. 3. Eight points were selected to estimate the effect of intensity overlap in terms of intensity. Table 2 shows the averaged values. The intensities range from 0 to 255, where 0 represents black and 255 represents white.

Through the green filter cube, the average peak intensities of the green and red particles are 250 and 46, respectively, leading to an overlap of 46/250=18%, while the overlap through the red filter cube is 2%.

In PIV analysis, intensity of energy is calculated to determine the most probable displacement, which can be defined as

$$E_1 = \iint_A I^2 dA, \quad (11)$$

where I is the intensity and A is the integration area. The intensity I can be approximated as a Gaussian function (Olsen and Adrian 2000)

$$I(r) = I_0 \exp\left(\frac{-4\beta^2 r^2}{d_e^2}\right), \quad (12)$$

where I_0 is the peak intensity, d_e is the particle image diameter, $\beta^2=3.67$ (Olsen and Adrian 2000). Substituting Eq. (12) into Eq. (11) and integrating from 0 to infinite, we find

$$E_1 = \frac{d_e^2 I_0^2}{16\beta^2}. \quad (13)$$

The peak intensity I_0 is listed in Table 2. The particle image diameter d_e can be calculated by (Adrian 1991)

$$d_e = \left[M^2 d_p^2 + d_s^2\right]^{\frac{1}{2}} \quad (14)$$

and

$$d_s = 1.22(1 + M)\lambda NA^{-1}, \quad (15)$$

where M is the magnification of the objective lens, d_p is the particle diameter, d_s is the point-spread function, λ is the light wavelength, and NA is the numerical aperture. With 20x, $NA=0.5$ objective lens, the image diameter of the 0.7 μm spheres emitting in the green ($\lambda=508\text{nm}$) is 29.6 μm , while that of the 1 μm red spheres ($\lambda=612\text{nm}$) is 37.2 μm . According to Eq. (13), the intensity energy ratio of the 0.7 μm particles to the 1 μm particles through the green filter cube is $(29.6/37.2)^2 \times (250/46)^2 = 19$, while that of the 0.7 μm particles to the 1 μm particles through the red filter cube is $(37.2/29.6)^2 \times (146/3)^2 = 3,741$. The cutoff of the filter schemes provides more than one order of magnitude in separation between the two different-sized particles. Therefore, the effect of overlap is sufficiently small and does not significantly affect the correlation functions.

For spherical particles, the magnitude of DEP force scales with radius cube (Eq. 2), while the magnitude of the

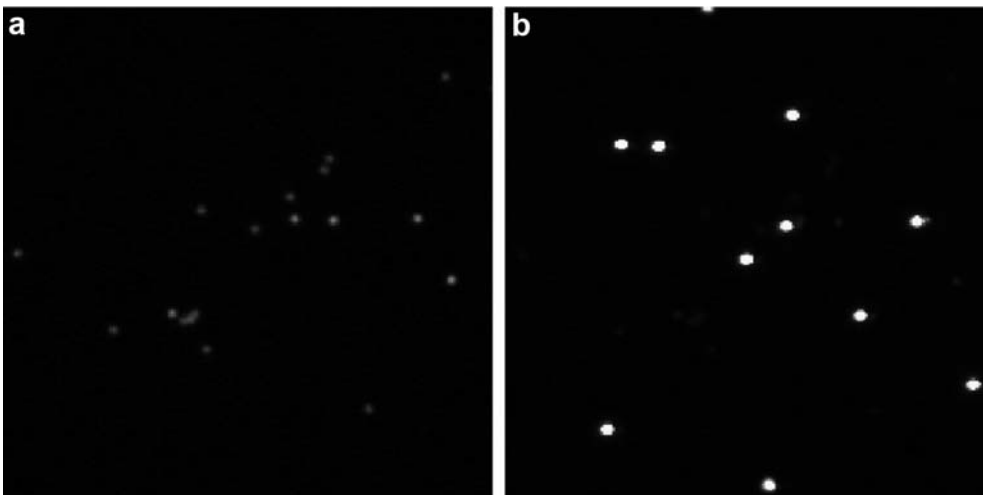


Fig. 3. Images of the same group of particles through two different filter cubes. **a** Particle image as viewed through the red filter cube. **b** Particle image as viewed through the green filter cube

Table 2. Intensity overlap

	Average peak intensity		Intensity ratio	Intensity energy ratio
	0.7 μm particle	1 μm particle		
Green filter cube	250	46	18%	19
Red filter cube	3	146	2%	3,741

hydrodynamic drag force scales linearly with radius (Eq. 4). Combining Eqs. (1), (2) and (4) gives the governing equations for two different-sized particles with similar electrical properties,

$$\varepsilon_m r_1^2 \text{Re}\{K\} \nabla |\vec{E}_{\text{rms}}|^2 + 3\mu(\vec{u}_f - \vec{u}_{p1}) = 0 \quad (16)$$

and

$$\varepsilon_m r_2^2 \text{Re}\{K\} \nabla |\vec{E}_{\text{rms}}|^2 + 3\mu(\vec{u}_f - \vec{u}_{p2}) = 0, \quad (17)$$

where u_{p1} and u_{p2} are the particle velocity fields, and r_1 and r_2 are the particle radii. The fluid velocity can be derived from the above two equations,

$$\vec{u}_f = \frac{\vec{u}_{p1} r_2^2 - \vec{u}_{p2} r_1^2}{r_2^2 - r_1^2}. \quad (18)$$

3.3

Microfluidic device

A microfluidic device was designed and fabricated to produce electrokinetically generated fluid motion in the observation plane. Figure 4 shows the test device. Two electrodes, separated by a 50 μm gap, were sandwiched between two glass wafers, forming a wedge-shaped 550 μm -deep microchannel. The glass covers were bonded to the electrodes by epoxy. Two plastic tubes were inserted between the two glass covers at the front and back sides to insert and extract the working fluid. The device was well sealed with epoxy and no leakage was observed. The electrodes were fabricated on a 550 μm -thick silicon wafer using

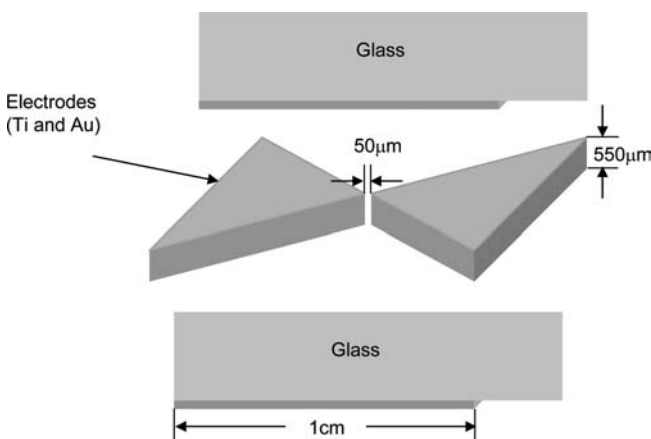


Fig. 4. Schematic diagram of the microfluidic device. An Si substrate is etched and Ti and Au is deposited on the Si substrate to form the electrode structure. The device is sandwiched by two glass wafers

PECVD, photolithography, deep RIE and e-beam evaporation. The microfluidic device was made at UCSB's Nanofabrication Facility. Figure 5 shows the fabrication process. By coating a silicon substructure with titanium and gold, we can produce electrodes that span the entire depth of the channel. Effective sidewall coverage was achieved with sample rotation through e-beam evaporation.

The characteristic dimension of the entire test section and the electrode structure is 1cm long and 550 μm thick. The test section top and bottom are made of glass, which is an electrical insulator, while the fluid is an electrical conductor. Therefore, the electric field is constrained to be two-dimensional. Since the electric field is two-dimensional and the test section is planar with a high aspect ratio, the resulting flow field will also be two-dimensional. The measurement was focused on the region near the electrode apex where the strong electric field can induce fluid motion and produce dielectrophoretic forces on particles.

A stabilized sweep generator (Model 22, Wavetek, San Diego, CA) is used to provide ac signals, a stereo power amplifier (P500, David Hafler, Pennsauken, NJ) to amplify the voltage, and a digital phosphor oscilloscope (TDS3032, Tektronix, Beaverton, OR) to measure the frequency and voltage applied on the microelectrodes. The applied voltage ranged from 11–14 V_{rms} , with a frequency $f=200$ kHz.

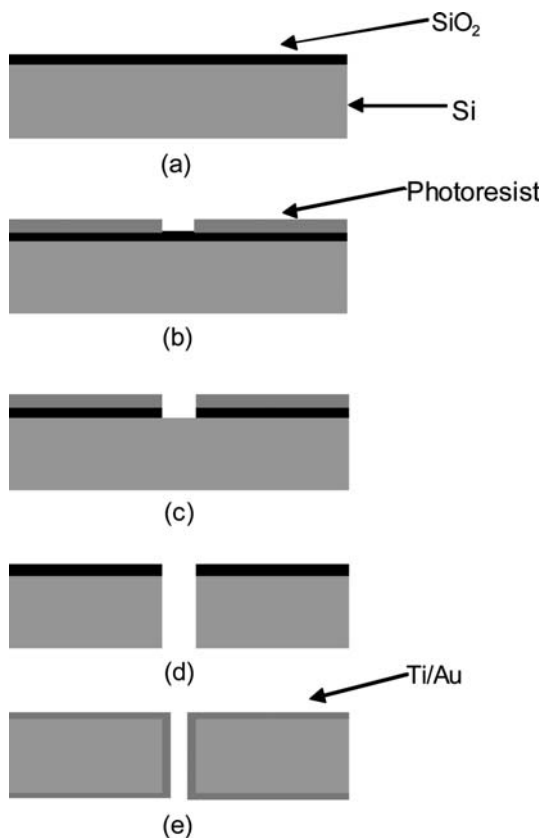


Fig. 5. Fabrication process for the electrode structure. a A 3 μm -thick layer of SiO_2 is deposited on a 550 μm -thick silicon wafer by PECVD. b The pattern of the wedge-shaped channel is transferred to the photoresist through photolithography. c The sample is soaked in BHF for 6 min to remove the exposed SiO_2 . d The wafer is etched using Deep RIE. e 500 \AA Ti and 4,000 \AA Au are deposited using an e-beam evaporator

The test suspension is contained in a microfluidic device, and the fluid velocity fields are determined using two-color μ -PIV.

The fluid is 8.5% (w/v) sucrose and 0.3% (w/v) dextrose sugar solution with the conductivity of 56mS/m. We assume the dielectric constant is near that of pure water, 79. The sugar solution is commonly used in DEP research because it is an isotonic buffer for cells. We chose this solution to remain consistent with the previous reported DEP experiments (Yang et al. 1999a, 1999b; Wang et al. 1998; Gascoyne et al. 1995). Fluorescent polystyrene particles of two size sets were dispersed in the fluid. The total volume fraction of the particles is 0.07%, with 0.02% for the 1 μ m and 0.05% for the 0.7 μ m particles. The particle concentrations were chosen to ensure that there were enough particles (1.4 red and 1.6 green) in each interrogation region to obtain valid time-averaged velocity measurements, while keeping the total volume fraction sufficiently small to minimize particle-particle interactions and to avoid adversely affecting the fluid. The particles have a dielectric constant of $\epsilon = 2.5$ and conductivity of $\sigma = 1.0 \times 10^{-14}$ mS/m (Lide et al. 2001). According to Eq. (2), the real part of the Clausius-Mossotti factor is $\text{Re}\{K\} = -0.5$ at a frequency of 200 kHz. Therefore the dielectrophoresis is negative, which tends to push the particles away from the intense electric fields located at the electrode apex.

4 Error analysis

The error in determining the fluid velocity with Eq. (18) can be evaluated by

$$\delta \vec{u}_f = \left(\left(\frac{\partial \vec{u}_f}{\partial \vec{u}_{p1}} \delta \vec{u}_{p1} \right)^2 + \left(\frac{\partial \vec{u}_f}{\partial \vec{u}_{p2}} \delta \vec{u}_{p2} \right)^2 + \left(\frac{\partial \vec{u}_f}{\partial r_1} \delta r_1 \right)^2 + \left(\frac{\partial \vec{u}_f}{\partial r_2} \delta r_2 \right)^2 \right)^{\frac{1}{2}}, \quad (19)$$

where $\delta \vec{u}_{p1}$ and $\delta \vec{u}_{p2}$ are the errors in measurement of the particle velocity fields, and δr_1 and δr_2 are the standard deviations of the particle radii. With the characteristic particle velocity $u_{p1} = u_{p2} = 100 \mu\text{m/s}$ and particle radii $r_1 = 0.5 \mu\text{m}$ and $r_2 = 0.35 \mu\text{m}$, the partial derivatives in the right-hand side can be calculated using Eq. (18), which are $\partial u_f / \partial u_{p1} = -0.96$, $\partial u_f / \partial u_{p2} = -1.96$, $\partial u_f / \partial r_1 = 75.3 \text{ s}^{-1}$ and $\partial u_f / \partial r_2 = -107.7 \text{ s}^{-1}$. When calculating $\partial u_f / \partial r_1$ and $\partial u_f / \partial r_2$, we assume that the difference in velocities between the particles and the fluid is about 10 $\mu\text{m/s}$. The percentage standard deviation is 5% and 3% for the 1 μm and 0.7 μm particles, respectively, (Duke Scientific Corp., Palo Alto, CA), giving $\delta r_1 = 0.025 \mu\text{m}$ and $\delta r_2 = 0.01 \mu\text{m}$. Therefore, the last two terms in the right-hand side of Eq. (19) are $3.5 \mu\text{m}^2/\text{s}^2$ and $1.2 \mu\text{m}^2/\text{s}^2$.

The measurement errors of particle velocity, $\delta \vec{u}_{p1}$ and $\delta \vec{u}_{p2}$, are primarily limited by Brownian motion and the diffraction limit of the recording optics.

To minimize the error due to Brownian motion, we used relatively large particles, 0.7 and 1 μm . The relative error due to the Brownian motion can be estimated by (Santiago et al. 1998)

$$\epsilon_B = \frac{1}{u} \sqrt{\frac{2D}{N\Delta t}}, \quad (20)$$

where u is the characteristic fluid velocity, D is the diffusion coefficient, N is the total number of particles involved in the velocity estimate, and Δt is the time interval between two successive images. The diffusion coefficient is given by (Santiago et al. 1998)

$$D = \frac{k_B T}{3\pi\mu d_p}, \quad (21)$$

where k_B is the Boltzmann constant, T is the absolute temperature, and d_p is the particle diameter.

In order to analyze the data recorded on the CCD camera, each particle frame is divided into many interrogation spots. Since Brownian motion is unbiased, the error can be reduced by averaging over a few particle images in one spot. Moreover, a series of particle frames are ensemble-averaged to further dampen the effects of Brownian motion.

The total number N is the product of the number of particle images used to obtain the estimate of velocity. The solid volume fraction of the 0.7 μm particles is 0.02%. One interrogation spot is a 10 $\mu\text{m} \times 10 \mu\text{m}$ area with a 15 μm -thick focus plane. The 15 μm measurement depth is estimated by using the technique described by Meinhart et al. (1999). The out-of-plane measurement thickness is estimated by determining the axial distance the objective lenses must be translated in order to cause a fixed particle to become sufficiently out of focus. Therefore, the total volume of 0.7 μm particles in one interrogation spot would be $0.3 \mu\text{m}^3$, i.e. 1.6 particles. There are 90 frames in total. So the total number of particles, N , is 144.

Applying the values $k_B = 1.38 \times 10^{-23} \text{ J/K}$, $T = 298 \text{ K}$, $\mu = 1.01 \times 10^{-3} \text{ Ns/m}^2$, $d_p = 0.7 \mu\text{m}$ to Eq. (21), we estimate the diffusion constant $D = 6.17 \times 10^{-13} \text{ m}^2/\text{s}$. With the fluid velocity 100 $\mu\text{m/s}$, and the time interval $\Delta t = 77 \text{ ms}$, the relative error due to Brownian motion is 0.33%, evaluated using Eq. (20).

The force balance between the particles and the fluid is described by Eq. (1). In the current experiment, we use relatively large particles to reduce the effects of Brownian motion. But large particles are subjected to DEP forces. In other words, we trade the stochastic error caused by Brownian motion for a deterministic error caused by DEP. However, the error resulting from DEP can be accounted for by the two different-sized particles using two-color μ -PIV.

The relative error due to uncertainty in particle displacement is given by

$$\epsilon_d = \frac{\delta x}{\Delta x}, \quad (22)$$

where δx is the uncertainty of particle image displacement due to diffraction and Δx is the particle displacement between two successive exposures. The uncertainty, δx , is related to the particle image diameter d_e , which is given by Eq. (14). The image diameter of 0.7 μm is 29.6 μm . Projected back to the flow field, the image diameter becomes

1.5 μm . We assume that if a particle is resolved over 3–4 pixels, the uncertainty of particle displacement is one-tenth of the particle image diameter (Prasad et al. 1992). Therefore, we assume the uncertainty in determining particle location due to diffraction is approximately $\delta x = 0.15\mu\text{m}$.

The characteristic fluid velocity is $u \sim 100\mu\text{m/s}$ and the time interval is 77ms, giving rise to a characteristic particle displacement $\Delta x = 7.7\mu\text{m}$. Using Eq. (22), we have the relative error due to diffraction for a single particle image of approximately $\varepsilon_d = 2.0\%$. Since we are averaging over $N = 144$ particles, we estimate the uncertainty is relatively to be $\varepsilon_D \approx \varepsilon_d / \sqrt{N} = 0.16\%$. The uncertainty in particle velocity can be conservatively estimated to be 1%, leading to $\delta u_{p1} = \delta u_{p2} \approx 1\mu\text{m/s}$. The first two terms in the right-hand side of Eq. (19) become 0.9 and $3.8\mu\text{m}^2/\text{s}^2$, respectively.

As a result of the previous calculation, the overall error in determining fluid velocity is $\delta u_f = 3.1\mu\text{m/s}$. Since the characteristic velocity is $100\mu\text{m/s}$, the uncertainty in determining fluid velocity using Eq. (18) is $\delta u_f / u_f \sim 3.1\%$.

5

Results and analysis

Figures 6 and 7 show 2-D velocity fields of ac electrokinetic particle and fluid flows in the wedge-shaped microchannel. The measurement domain is a $415\mu\text{m} \times 415\mu\text{m}$ square, corresponding to 1024×1024 pixels on the CCD camera. This measurement domain is $150\mu\text{m}$ below the top glass wafer. The applied voltage is $12V_{\text{rms}}$ with a frequency $f = 200\text{kHz}$, producing a non-uniform electric field across the wedge-shaped channel. Under the influence of this electric field, the particles were subjected to Stokes' drag and dielectrophoresis. Figure 6 shows the velocity fields of the $1\mu\text{m}$ and $0.7\mu\text{m}$ fluorescent spherical particles, respectively. These two vector fields are raw PIV data resulting from averaging over 90 continuous images taken at a rate of 13 fps, without smoothing or removing erroneous velocity vectors. Near the electrode apex, there are large gradients in the electric field. However, this is a stagnation point for the fluid, and the electrothermal force is relatively small. This is confirmed by numerical simulations (not reported here).

The velocity vectors near the electrode tips were not available because the fluorescent particles agglomerated due to particle-particle interactions, making it impossible to image individual particles. Furthermore, in this region, some particles aligned in chains under the effect of the applied electric field, violating the requirement of low particle density.

Figure 7 is the velocity field of electrokinetic fluid flow, determined uniquely from the two particle velocity fields using Eq. (18), without a priori knowledge of the 2-D electric field, the fluid properties, or the Clausius-Mossotti factor. Figures 6a and 6b appears qualitatively similar to Fig. 7. However, the quantitative accuracy of the $\mu\text{-PIV}$ technique produces clear and measurable differences between these two velocity fields.

Figure 8 shows the direction and magnitude (within a constant) of the negative dielectrophoretic force on the

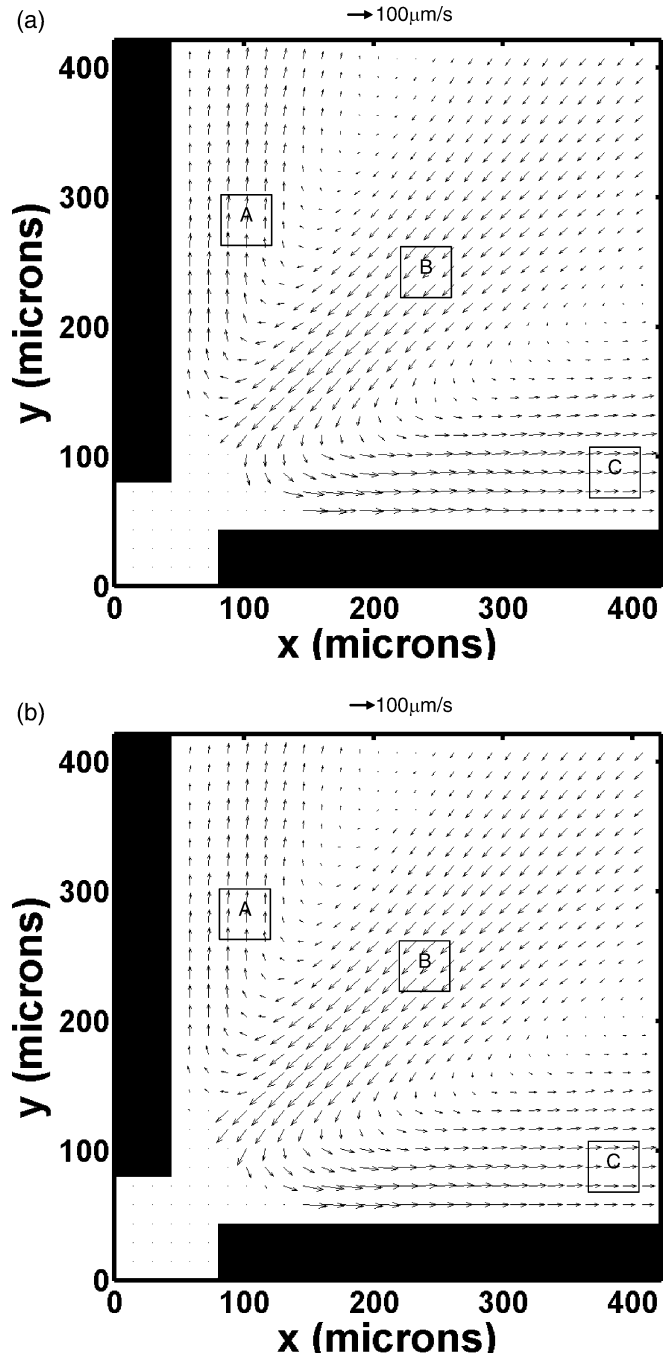


Fig. 6. Particle velocity fields obtained using two-color $\mu\text{-PIV}$. **a** The velocity field of the $1\mu\text{m}$ -diameter polystyrene particles; **b** the velocity of the $0.7\mu\text{m}$ -diameter polystyrene particles. The regions A, B and C are characteristic regions of the flow. The black rectangles represent the electrodes. The applied voltage is $12 V_{\text{rms}}$ at a frequency of 200 kHz. These are raw data, i.e. no smoothing was applied

particles, calculated according to Eq. (2) using FEMLAB finite element software (Comsol Inc., Burlington, MA). The similarity between the fluid and particle velocity fields (Figs. 6a, 6b and 7) indicates that particles closely follow the fluid flow, and that while the DEP force is finite, it does not dominate the particle motion. If the DEP force were dominant, the particles would move away from the electrode tips in the directions shown in Fig. 8.

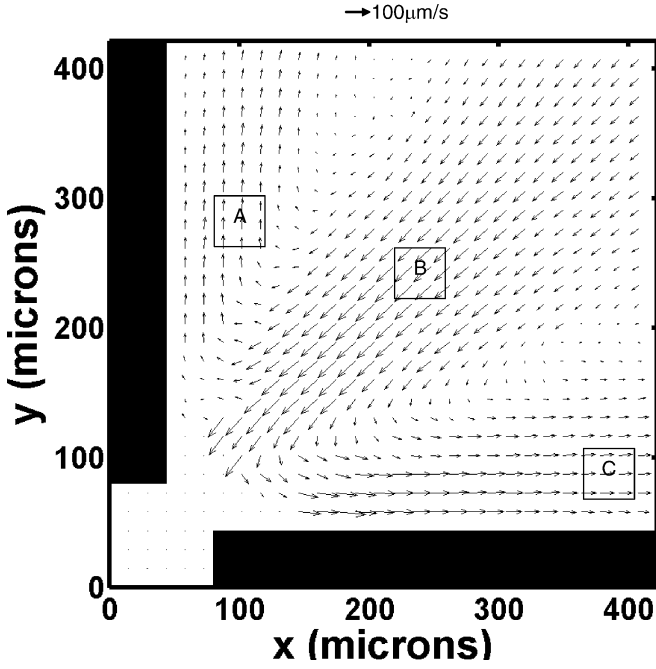


Fig. 7. The fluid velocity field, determined from the two particle velocity fields shown in Fig. 5 using Eq. (18). The applied voltage is $12V_{\text{rms}}$ at a frequency of 200kHz. In the middle of the test device, fluid is drawn towards the electrode apex. Near the electrodes, the fluid moves away from the apex

Although the particle and fluid flows are similar to one another, differences do exist. These differences are measured quantitatively using μ -PIV. In Figs. 6, 7, 8, the three regions A, B and C were selected as characteristic regions

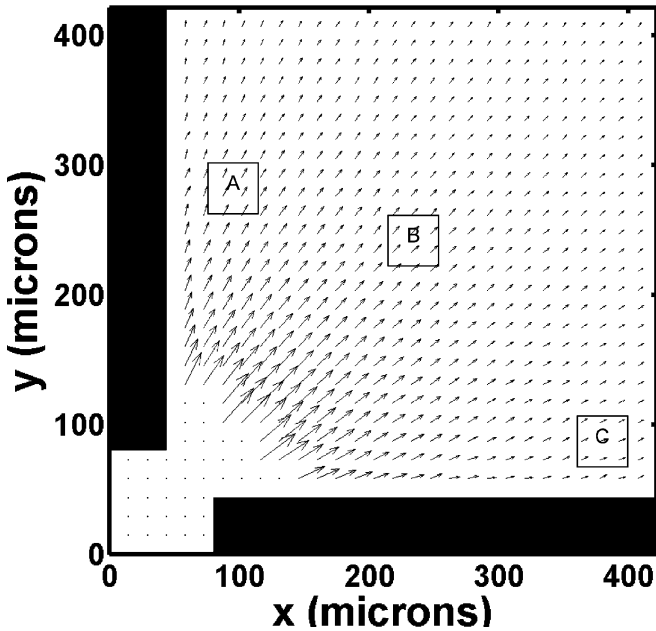


Fig. 8. Numerical simulation of dielectrophoretic force field. Negative DEP will tend to move particles away from the electrode tips (i.e. away from high electric field intensity). The dielectrophoresis near the electrode tips are not shown because their magnitudes are too large

Table 3. Velocity in each region ($\mu\text{m/s}$), for voltage $12V_{\text{rms}}$, $f=200$ kHz

	A	B	C
u_{p1} ($1\mu\text{m}$)	65	107	88
u_{p2} ($0.7\mu\text{m}$)	59	121	85
u_f	54	135	82

of the flow. Regions A and C are near the electrodes, and region B at the center of the flow. The magnitudes of the velocity vectors within each region are averaged and shown in Table 3, where u_{p1} is the velocity of $1\mu\text{m}$ particles, u_{p2} the velocity of $0.7\mu\text{m}$ particles, and u_f the fluid velocity.

Table 3 shows that the particles are influenced by both fluid flow and dielectrophoresis. The particle velocity is similar to the corresponding fluid velocity in all the three regions, suggesting that the particle motion closely follows the fluid motion. However, there is a slight difference in velocity between the particles and the fluid, suggesting that dielectrophoresis has a small effect. According to Figs. 7 and 8, the fluid flow is in nearly the same direction as dielectrophoresis in regions A and C. Therefore all the particles are moving faster than the fluid. At region B, dielectrophoretic forces point opposite to the fluid flow, leading to the particles moving slower than the fluid. Table 3 also shows that the velocity of the larger particles is larger than that of the smaller particles at regions A and C, and the reverse is true at region B. This can be explained with Eq. (2), which indicates that the magnitude of the dielectrophoretic force scales with the cube of the particle radius. Accordingly, the $1\mu\text{m}$ particles experience a dielectrophoretic force three times larger than the $0.7\mu\text{m}$ particles, giving rise to the fact that the larger particles deviate from the fluid flow more than the smaller particles.

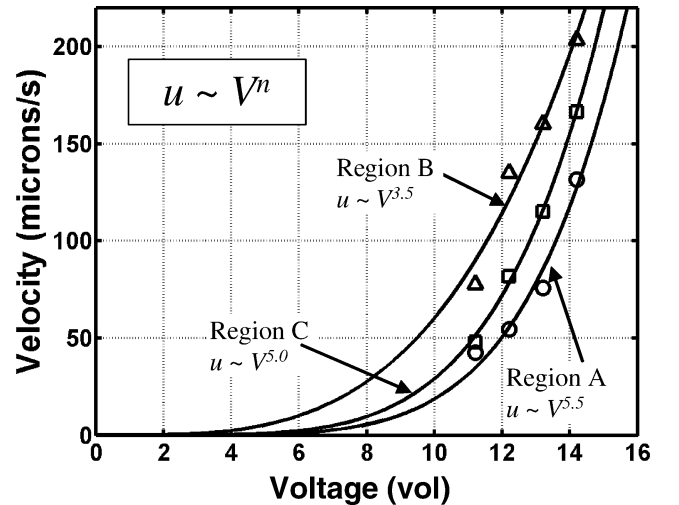


Fig. 9. Fluid velocity at different voltages. O represents averaged fluid velocity in region A, Δ in region B and \square in region C. Fluid velocity u is assumed proportional to V^n , and n is found by the fitting curves

The flow pattern shown in Fig. 7 is similar to that caused by the electrothermal effect (Ramos et al. 1998; Meinhart and Wang 2001), and by ac electroosmosis (Ramos et al. 1998, 2000; Green et al. 2000). According to Eqs. (9) and (10), the fluid velocity scales with $u_f \sim V^4$ for electrothermally driven flow, and with $u_f \sim V^2$ for ac electroosmosis flow.

To determine which effect is dominant, we assume the fluid velocity obeys a power law, such that $u_f \sim V^n$. Fluid velocity in regions A, B and C were measured over a range of applied voltages, $V=2-14V_{\text{rms}}$, and n was found by fitting curves. Figure 9 shows the variation of the velocity with the applied voltage. The curve fitting reveals that at region B, around the center of the geometry, $n \approx 3.5$, which is close to 4, seeming to indicate dominance of electrothermally generated motion here. At regions A and C, near the electrodes, $n \approx 5-5.5$, which is a stronger dependence on voltage than either phenomena predicts. The fluid near the electrodes may be driven by a combination of the electrothermal effect and ac electroosmosis. In addition, there may be higher order effects occurring in the electric double layers, which are not accounted for in the simplified model developed by Ramos et al. (1998).

6

Conclusions

Decoupling of fluid velocity fields from observed particle velocity fields through two-color μ -PIV in a 2-D wedge device allows the study of the various electrokinetic phenomena which affect particle and fluid motion: dielectrophoretic force on particles, ac electroosmotic force on the fluid surface, and electrothermal force on the fluid body.

In the current experiment, the difference between particle and fluid velocity fields, as a result of DEP force on particles, was small, indicating that DEP is not dominant in this regime. The differences that did occur, however, agree qualitatively with the DEP force estimated based on fluid and particle properties.

The fluid velocity fields at different applied voltages were measured and compared in an effort to find the relation between the fluid velocity and the applied voltage. For the current experimental conditions, the fluid velocity scales approximately with voltage to an exponential power of $n \sim 3.5-5.5$. This suggests that for the current experiments, electrokinetically generated fluid motion may result from both the electrothermal effect and ac electroosmosis, and that the electrothermal effect is dominant in the bulk fluid.

References

- Adrian RJ (1991) Particle-imaging techniques for experimental fluid mechanics. *Ann Rev Fluid Mech* 23:261-304
- Bakewell D, Hughes M, Milner J, Morgan H (1998) Dielectrophoretic manipulation of avidin and DNA. *Proceedings of the 20th Annual International Conference of the IEEE Engineering in Medicine and Biology Society* 20(2):1079-1082
- Brown ABD, Smith CG, Rennie AR (2001) Pumping of water with ac electric fields applied to asymmetric pairs of microelectrodes. *Phys Rev E* 63, pp 016305/1-8
- Cummings E (2000) An image processing and optimal nonlinear filtering technique for particle image velocimetry of microflows. *Exp Fluids (Suppl)* 29(7):42-50
- Deen W (1998) *Analysis of transport phenomena*. Oxford University Press, New York
- Gascoyne PRC, Wang XB, Huang Y, Becker FF (1995) Dielectrophoretic separation of cancer cells from blood. *Conference Record of the 1995 IEEE Industry Applications Conference, IEEE*, vol 2, pp 1366-73
- Green N, Ramos A, Gonzalez A, Morgan H, Castellanos A (2000) Fluid flow induced by nonuniform ac electric fields in electrolytes on microelectrodes, I. Experimental measurements. *Phys Rev E* 61(4):4011-4018
- Jones T (1995) *Electromechanics of particles*. Cambridge University Press, New York
- Kundu PK, Cohen IM (2002) *Fluid Mechanics*, 2nd edn. Academic Press, New York
- Lide DR (2001) *CRC Handbook of chemistry and physics*, 82nd edn. CRC Press, Boca Raton, FL
- Meinhart C, Wang D (2001) Accurate measurement of dielectrophoretic (DEP) mobility of particles and macromolecules. *Proceedings of μ -TAS 2001*, Monterrey, CA, October 21-25, 2001
- Meinhart C, Wereley S, Santiago J (1999) PIV measurements of a microchannel flow. *Exp Fluids* 27(5):414-419
- Meinhart C, Wereley S, Gray M (2000a) Volume illumination for two-dimensional particle image velocimetry. *Meas Sci Technol* 11(6):809-814
- Meinhart C, Wereley S, Santiago J (2000b) A PIV algorithm for estimating time-averaged velocity fields. *J Fluids Eng* 122(2):285-289
- Meinhart C, Wang D, Turner K (2003) Measurement of ac electrokinetic flows. *Biomed Microdevices* 5(2):139-145
- Morgan H, Green N (2003) *AC electrokinetics: colloids and nanoparticles*, Research Studies Press Ltd., Baldock, Hertfordshire, England
- Morgan H, Hughes M, Green N (1999) Separation of submicron bioparticles by dielectrophoresis. *Biophys J* 77:516-525
- Olsen MG, Adrian RJ (2000) Out-of-focus effects on particle image visibility and correlation in microscopic particle image velocimetry. *Exp Fluids* 29 (Suppl S):166-174
- Prasad AK, Adrian RJ, Landreth CC, Offutt PW (1992) Effect of resolution on the speed and accuracy of particle image velocimetry interrogation. *Exp Fluids* 13:105-116
- Ramos A, Morgan H, Green N, Castellanos A (1998) AC electrokinetics: a review of forces in microelectrode structures. *J Phys D Appl Phys* 31:2338-2353
- Ramos A, Gonzalez A, Green N, Castellanos A, Morgan H (2000) Fluid flow induced by nonuniform ac electric fields in electrolytes on microelectrodes, II. A linear double-layer analysis. *Phys Rev E* 61(4):4019-4028
- Santiago J, Wereley S, Meinhart C, Beebe D, Adrian R (1998) A particle image velocimetry system for microfluidics. *Exp Fluids* 25:316-319
- Sigurdson M, Meinhart C, Wang D, Liu X, Feng J, Krishnamoorthy S, Makhijani V (2002) Transport enhancement in tunable laser cavity sensor. *ASME-IMECE'02 MEMS Symposium*, New Orleans, LA, Nov. 17-22, 2002
- Studeer V, Pepin A, Chen Y, Ajdari A (2002) Fabrication of microfluidic devices for ac electrokinetic fluid pumping. *Microelectron Eng* (61-62):915-920
- Wang XB, Vykoukal J, Becker FF, Gascoyne PRC (1998) Separation of polystyrene microbeads using dielectrophoretic/gravitational field-flow-fractionation. *Biophys J* 74(5):2689-701
- Wong PK, Chen CY, Wang TH, Ho CM (2003a) An ac electroosmotic processor for biomolecules, *TRANSDUCERS '03. 12th International Conference on Solid-State Sensors, Actuators and Microsystems. Digest of Technical Papers. IEEE*. vol 1, pp 20-3. Piscataway, NJ, USA
- Wong PK, Wang JTH, Deval JH, Ho CM (2003b) Electrokinetics in microdevices for biotechnology applications, *IEEE/ASME Transactions on Mechatronics*

Yang J, Huang Y, Wang X, Wang XB, Becker F, Gascoyne PRC (1999a) Dielectric properties of human leukocyte subpopulations determined by electrorotation as a cell separation criterion. *Biophys J* 76:3307-3314

Yang J, Huang Y, Wang XB, Becker F, Gascoyne PRC (1999b) Cell separation on microfabricated electrodes using dielectrophoretic/gravitational field-flow-fractionation. *Anal Chem* 71(5):911-918